

Tunable Electronic Properties of Multilayer Phosphorene and Its Nanoribbons

S. Soleimanikahnoj* and I. Knezevic†

*Department of Electrical and Computer Engineering,
University of Wisconsin-Madison, Madison, WI 53706, USA*

(Dated: May 1, 2022)

We study the effects of a vertical electric field on the electronic band structure and transport in multilayer phosphorene and its nanoribbons. We find a massive-to-massless Dirac fermion transition along the armchair direction at a critical field E_c at which the gap closes. This transition is observable in quantum Hall measurements, as the power-law dependence of the Landau-level energy on the magnetic field goes from $\sim (n + 1/2)B$ below E_c , to $\sim [(n + 1/2)B]^{2/3}$ at E_c , to $\sim [(n + 1/2)B]^{1/2}$ above E_c . Multilayer phosphorene nanoribbons (PNRs) have edge states that govern electrical conduction. We propose a dual-edge-gate PNR structure that works as a quantum switch.

I. INTRODUCTION

Black phosphorus (BP) is a thermodynamically stable allotrope of phosphorus with a layered structure. The layers of covalently bonded atoms are held together by the van der Waals interaction. Similar to obtaining graphene from graphite by mechanical exfoliation, BP can be isolated to a few layers [1, 2]. The resulting structure is a recent addition to the family of two-dimensional (2D) materials called multilayer phosphorene. Monolayer phosphorene has a direct band gap of 1.45 eV [2]. In multilayer phosphorene, the gap decreases with increasing number of layers owing to relatively strong van der Waals interactions between the layers and remains direct [3]. This makes phosphorene a promising candidate for electronic and optical applications [4–10]. Moreover, the phosphorene crystal structure is highly anisotropic, which gives rise to phenomena such as anisotropic electronic and thermal transport [8, 11–15], linear dichroism [8, 13], and anisotropic plasmons [16]. Additionally, owing to its heavily puckered structure, phosphorene is highly tunable by strain [11, 17] and electric field [12, 18]. In particular, applying an electric field normal to the layers reduces the band gap, leading to a transition from a moderate-gap semiconductor to a semimetal [19]. Applying an electric field also leads to the emergence of more exotic features of phosphorene, including nontrivial topological phases [20–22]. However, the transition of the Landau levels (LLs) under the influence of electric field as a trademark of the topological phase transition has not been fully understood. Furthermore, little is known about the possible practical use of electric field modulation in tuning the electronic characteristics of nanostructures based on phosphorene.

In this paper, we investigate the effects of a vertical electric field on the electronic properties (band structure and electronic transport) of multilayer phosphorene and its nanoribbons. In multilayer phosphorene at low fields,

electrons with momenta in the zigzag direction [Fig. 1(a)] have parabolic bands, but in the armchair direction they behave as massive Dirac fermions with a gap-dependent effective mass. At a critical electric field E_c , the gap closes, and electrons exhibit a massive-to-massless Dirac fermion transition. Above E_c , there are two Dirac points, and the band structure is that of anisotropic massless Dirac fermions. This continuous massive-to-massless Dirac fermion transition could be observed in Hall measurements, as the LL energy dependence on the magnetic field would change from linear below E_c , to the novel 2/3-power at E_c , to the square-root dependence above E_c . In phosphorene nanoribbons (PNRs), we show that there are twofold-degenerate bands within the bulk gap, which govern electronic transport. The associated wave functions are localized near the ribbon edges. We propose a dual-edge-gate structure that affects these midgap states and drives the conducting-to-insulating transition in PNRs, thus enabling field-effect transistor action compatible with modern nanoelectronics, and potentially leading to new PNR-based devices.

II. THE TIGHT-BINDING MODEL

The band structure of multilayer phosphorene is described by a tight-binding (TB) Hamiltonian

$$H = \sum_{i,j} t_{i,j} c_i^\dagger c_j, \quad (1)$$

which was parametrized on the basis of first-principles calculation within the GW_0 approximation [23, 24]. As the TB parametrization was benchmarked for mono-, bi- and trilayers, we restrict our study here to these three systems, but note that TB may be suitable for larger multilayers, as well. A phosphorene monolayer contains two sublayers in a puckered structure and has four atoms per unit cell. Each additional layer brings four more atoms to the unit cell (see the structure of bilayer phosphorene in Fig. 1), with odd-numbered layers aligned with other odd-numbered ones, and analogously for even-numbered layers. A unit cell for bilayer phosphorene is denoted by

* soleimanikah@wisc.edu

† iknezevic@wisc.edu

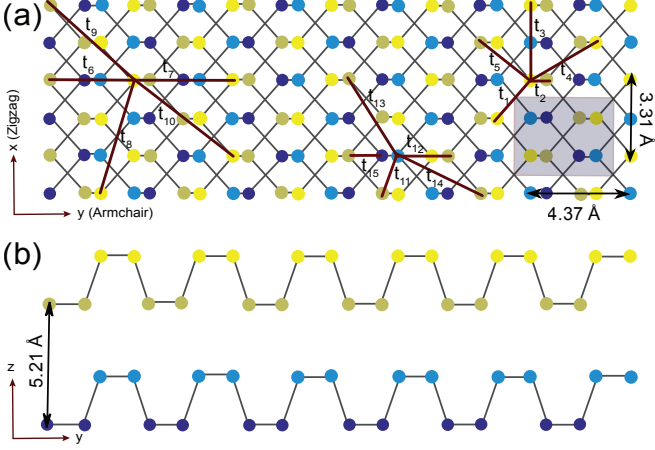


FIG. 1. Schematic of bilayer phosphorene. (a) Top view. (b) side view. The left and the right edges are zigzag, while the top and bottom edges are armchair. Yellow (blue) circles are the phosphorene atoms in the upper (lower) layer while the atoms in the upper (lower) sublayer are portrayed a bright (dark) color. The gray rectangle denotes the unit cell of bilayer phosphorene. Higher multilayer systems will have the unit cell with the same top view and with additional 4 atoms per layer.

TABLE I. Hopping parameters for the tight-binding Hamiltonian in Eq. (1). $i = 1 - 10$ are intralayer and $i = 11 - 15$ are interlayer coupling terms.

i	t_i (eV)	d_i (Å)	i	t_i (eV)	d_i (Å)	i	t_i (eV)	d_i (Å)
1	-1.486	2.22	6	+0.186	4.23	11	+0.524	3.60
2	+3.379	2.24	7	-0.063	4.37	12	+0.180	3.81
3	-0.252	3.31	8	+0.101	5.18	13	-0.123	5.05
4	-0.071	3.34	9	-0.042	5.37	14	-0.168	5.08
5	+0.019	3.47	10	+0.073	5.49	15	+0.005	5.44

the shaded box in Fig. 1(a). In the nearest-neighbor approximation, there are fifteen relevant tight-binding hopping parameters (Table I), ten intralayer and four interlayer. The multilayer phosphorene structure is highly anisotropic. Cutting phosphorene in the (horizontal) y direction (see Fig. 1) would result in an armchair edge, while cutting along the (vertical) x direction would result in a zigzag edge. We refer to the y -direction as armchair and the x -direction as zigzag.

III. PHOSPHORENE BANDSTRUCTURE AND FIELD MODULATION

The band structure of trilayer phosphorene is depicted in Fig. 2(a); note the rectangular Brillouin zone (BZ) and its high-symmetry X and Y points along the x and y directions. The band gap, E_g , is at the Γ point and has a value of 0.85 eV. Along the zigzag direction, both the

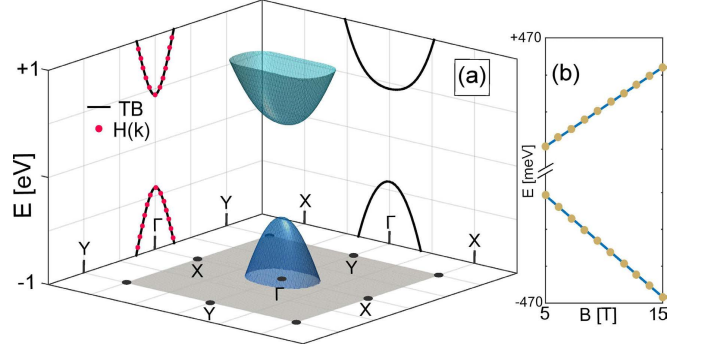


FIG. 2. (a) Band structure of unbiased trilayer phosphorene over the first Brillouin zone. Cuts normal to (10) and (01) through the Dirac point are projected onto the side walls, with the high-symmetry Γ , X , and Y points denoted. The solid lines are from TB, the red dotted line from the low-energy two-band Hamiltonian (2). (b) Magnetic field dependence of CB and VB for trilayer phosphorene in absence of electric field bias. The linear blue lines are fitted to the yellow dots obtained from the Harper's equation.

conduction band (CB) and the valence band (VB) show quadratic dependencies on the wave vector \mathbf{k} [Fig. 2(a)]. We calculate the effective masses of $m_c = 3.18m_0$ (CB) and $m_v = 0.84m_0$ (VB), where m_0 is the free-electron rest mass. In the armchair direction, however, the dispersion has an asymptotic linear trend. To describe this highly anisotropic band structure near the band gap, we propose a low-energy two-band Hamiltonian as

$$H(\mathbf{k}) = \mathbf{h}(\mathbf{k}) \cdot \boldsymbol{\sigma}, \quad \mathbf{h}(\mathbf{k}) = \left[\frac{\hbar^2 k_x^2}{2m_{c(v)}} + \frac{E_g}{2}, \hbar v_y k_y, 0 \right]. \quad (2)$$

Here, $\boldsymbol{\sigma}$ are the Pauli matrices, m_c and m_v are the effective masses in the zigzag direction, and $v_y = 7.4 \times 10^5$ m/s is the Fermi velocity in the armchair direction. In Fig. 2(b), we see that the fit from this effective two-band Hamiltonian (red dots) agrees very well with the CB and VB dispersions obtained by TB (solid curve) within ± 1 eV of midgap. Finding the dispersion for $k_x = 0$ from the two-band Hamiltonian (2) leads to

$$E(0, k_y) = \pm \sqrt{(\hbar k_y v_y)^2 + \left(\frac{E_g}{2} \right)^2}. \quad (3)$$

This is a characteristic dispersion of massive relativistic particles [25], where E_g plays the role of rest energy. Upon employing the relativistic definition of the effective mass as $m_y = \hbar^2 k (dE/dk_y)^{-1}$, we obtain an effective mass for both CB and VB in the armchair direction to be $m_y = E_g/2v_y^2 = 0.12m_0$, a value close to the experimentally obtained $0.08m_0$ [19], which could not be explained previously based on the parabolic approximation. Thus, it is important to consider electrons in the armchair direction as massive Dirac fermions.

Since unbiased phosphorene is a conventional 2D electron gas, CB and VB are expected to have a linear dependence on an applied vertical magnetic field [26–28]. In order to check this hypothesis, magnetic field is incorporated in the tight-binding model through Peierls substitution, which adds a phase to the hopping term between any two sites,

$$t_{i,j} \rightarrow t_{i,j} e^{\frac{e}{\hbar} \int_{R_i}^{R_j} \mathbf{A} \cdot d\mathbf{l}}, \quad (4)$$

where $\mathbf{A} = (-By, 0, 0)$ is the vector potential and B is the magnitude of the magnetic induction in z -direction. By this substitution, one will arrive at Harper's equation [29–32], and LLs are obtained by numerical calculation of its eigenvalues. For unbiased trilayer phosphorene, the LLs were calculated at various magnetic fields. The bands corresponding to the CB and VB are shown in Fig. 2(b). Predictably, CB and VB change linearly as a function of magnetic field strength.

Next, we extend our model to the case of a vertical electric field E_z [applied normal to the layers, i.e., in the z -direction in Fig. 1(a)]. In the TB calculations, E_z is accounted for by assuming a linear potential drop across the structure extending from $-h/2$ to $h/2$ (h is the thickness): a potential energy $V_i = eE_z(-h/2 + z_i)$ is added to the diagonal terms of the TB Hamiltonian in Eq. (1) according to i -th atom's z coordinate. Figure 3(c) shows that, as E_z increases, the CB and VB shift toward each other due to the Stark effect. The band gap closes at a critical electric field, E_c , [19] which decreases with increasing number of layers: $E_c \simeq 0.17 \text{ V/Å}$ for bilayer (also reported in 33) and $E_c \simeq 0.15 \text{ V/Å}$ for trilayer phosphorene. The full band structure of trilayer phosphorene at E_c is depicted in Fig. 3(a). Electric field affects the curvature of the parabolic CB and VB bands along the zigzag direction [Fig. 3(b)]: m_c (m_v) decreases (increases) with increasing E_z , but $m_v < m_c$ for all values of E_z , in keeping with the high hole mobility reported in experiment [2].

Application of the vertical electric field and the corresponding gap reduction have a strong effect on dispersion in the armchair direction: as $m_y \propto E_g$, m_y drops with increasing E_z and reaches zero at E_c [Fig. 3(c)]. Therefore, there is a smooth transition from massive to massless Dirac fermions in the armchair direction under a vertical electric field. At E_c , the dispersion of CB and VB near the gap becomes

$$E(\mathbf{k}) = \pm \sqrt{(\hbar k_y v_y)^2 + \left(\frac{\hbar^2 k_x^2}{2m_{c(v)}}\right)^2}. \quad (5)$$

Owing to the anisotropic dispersion at the critical electric field – massless Dirac [Eq. (5)] along y , parabolic along x – the electron density of states (DOS) has a peculiar energy dependence: $\rho(E) \sim \frac{m}{v_y} \sqrt{E}$. [34] If such an electron system were placed in a uniform vertical magnetic field B , it would exhibit a unique dependence of the LL

energy on the B field (stemming from the square-root energy dependence of the DOS [35]) that has never before been observed in experiment:

$$E_n \sim \left[\left(n + \frac{1}{2} \right) B \right]^{2/3}, \quad (6)$$

We obtained this dependence [see Fig. 3(d)] by numerically solving Harper's equation, as described earlier. The 2/3-power dependence is distinct from the linear dispersion in two-dimensional electron gases, $E_n \sim (n + \frac{1}{2}) B$ [shown in Fig. 2(b)], and from the square-root dependence characteristic of Dirac fermions, $E_n \sim \sqrt{(n + \frac{1}{2}) B}$. Biased multilayer phosphorene would be the first realization of this LL dispersion in a real material, though the phenomenon was thoroughly investigated on a parametric honeycomb lattice [36–38]. While Yaun *et al* [33], recently investigated LLs in perpendicular electric fields, they did not solve the Harper's equation [29–32] in an extended system, as we did, and thus did not note this peculiar behavior at E_c . We propose an extension to experiment [19], where the gap is closed via doping and mimics applying E_c : a measurement of the Hall conductance at this condition would experimentally confirm the peculiar form (6) of the LL B -field dependence.

Increasing the electric field beyond the critical value ($E_z > E_c$) splits the Dirac point into two. The Dirac points (Δ_X) move away from the Γ point along the X direction as a function of electric field [see Fig. 4(a)]. In the low-energy, two-band Hamiltonian (2), $\mathbf{h}(\mathbf{k})$ takes the form

$$\mathbf{h}(\mathbf{k}) = \left[\frac{\hbar^2 k_x^2}{2m_{c(v)}} - \frac{E_{inv}}{2}, \hbar v_y k_y, 0 \right], \quad (7)$$

where E_{inv} is the value of the inverted gap shown in Fig. 4(a). At each Dirac point, the Hamiltonian can be expanded in terms of $\mathbf{q} = \mathbf{k} - \mathbf{k}_{\Delta_X}$, which gives us the low-energy form $H(\mathbf{q}) = \hbar v_x q_x + \hbar v_y q_y$, a generic Dirac Hamiltonian with anisotropic Fermi velocity $v_{x,c(v)} = \sqrt{E_{inv}/m_{c(v)}}$ and ultimately the dispersion relation

$$E(\mathbf{q}) = \sqrt{(\hbar v_x q_x)^2 + (\hbar v_y q_y)^2} \quad (8)$$

Based on this dispersion, the Berry phase, Λ , can be calculated by integrating the Berry potential, $\nabla \Lambda = \frac{\hbar^2 v_x v_y}{2E(\mathbf{q})^2} [-q_y, q_x]$, over a closed path around each Dirac point; the integration path chosen here is a circle around each Dirac point, depicted in Fig. 4(a). $\Lambda = \pm\pi$ is obtained from both the two-band low-energy and TB Hamiltonians. [39, 40] This means that electrons in biased multilayer phosphorene carry an extra degree of freedom called the pseudospin. Dirac fermions exhibit unconventional quantum Hall effect, where LLs vary with B as $E_n \sim \sqrt{(n + \frac{1}{2}) B}$. [33, 41]. Magnetic field dependency of CB and VB of multilayer phosphorene biased

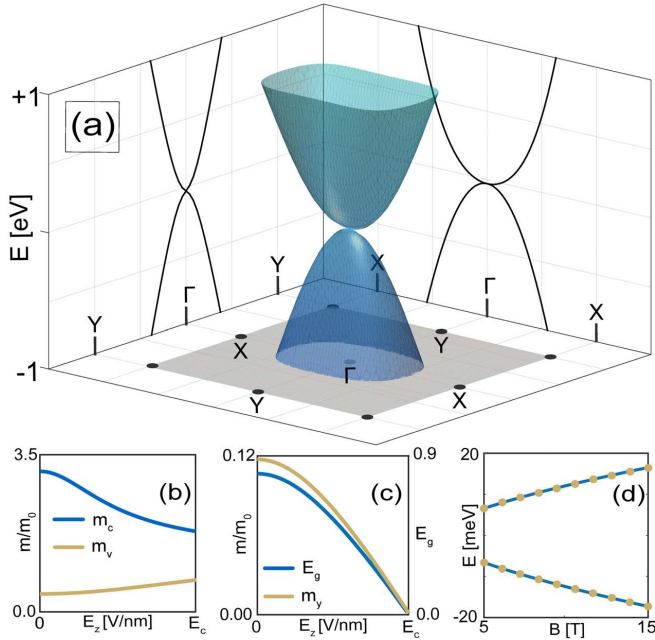


FIG. 3. (a) Band structure of biased trilayer phosphorene at the critical electric field ($E_z = E_c$). (b) Effective mass in the conduction and valence bands as a function of electric field along the zigzag direction. (c) Band gap and relativistic effective mass (both CB and VB) in the armchair direction versus electric field. (d) Energy of the lowest LL in the CB and VB versus magnetic field B , obtained by solving Harper's equation (dots). Solid lines are fits based on Eq. (6).

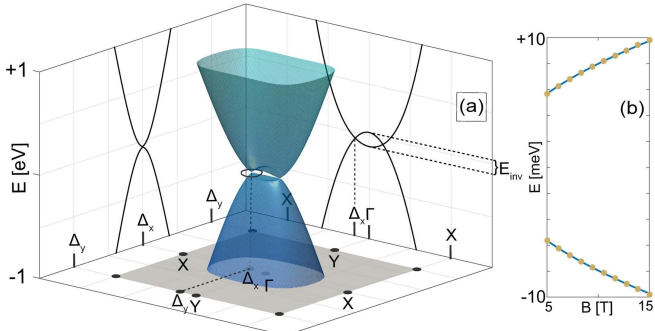


FIG. 4. (a) Band structure of biased trilayer phosphorene at $E_z > E_c$. A pair of Dirac points appear in the band structure (Δ_x). (b) CB and VB (yellow dots) as a function of magnetic field obtained from diagonalization of Harper's equation at ($E_z > E_c$). The data is fitted with the square root power law of Dirac fermions (blue lines).

at $E_z > E_c$ are shown in Figs. 4(b). As can be seen, both CB and VB (yellow circles) follow the square root power law of Dirac fermions (blue lines).

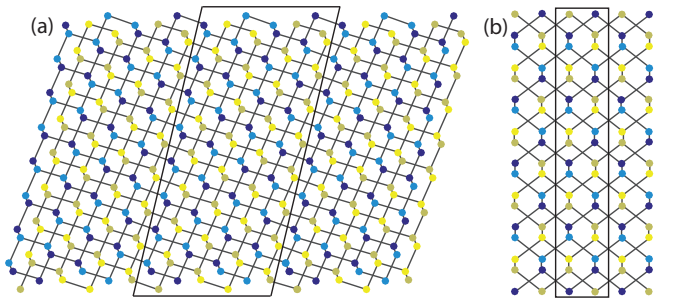


FIG. 5. Crystal structure of bilayer skewed-armchair (a) and zigzag (b) PNRs. Corresponding unit cells are outlined by the solid line boxes.

IV. METALLIC PHOSPHORENE NANORIBBONS

In order to obtain metallic PNRs, we can choose to confine multilayer phosphorene along two different directions, which results in skewed-armchair and zigzag PNRs shown in Figs. 5(a) and 5(b), respectively. Other types of PNRs are disregarded due to insulating behavior [42–44]. The band structures of mono-, bi-, and trilayer zigzag PNRs are shown in Figs. 6(a)–(c) and those corresponding to skewed-armchair PNRs are shown in Figs. 6(d)–6(f), respectively. One can see the presence of midgap bands (red curves) completely detached from the bulk bands (shown in blue). For zigzag PNRs, each layer of phosphorene contributes one band of twofold-degenerate midgap states, making a total of two, four, six midgap states for mono-, bi- and trilayer PNRs, respectively. However in case of skewed-armchair PNRs, each layer provides two, twofold-degenerate midgap states. As a result, a total of four, eight, twelve midgap bands are present for mono-, bi- and trilayer skewed-armchair PNRs, respectively.

In the absence of a vertical electric field, zigzag PNRs are metallic since the Fermi level passes through all midgap bands and is far from the bulk states. In a similar manner, metallicity of skewed-armchair PNRs is caused by the two midgap states closest to the Fermi level without any contribution from the bulk states [see Figs. 6(d)–6(f)]. Therefore, near-equilibrium electronic transport in metallic PNRs is governed by midgap states. In Figs. 6(g) and 6(h), we plot the probability density for two $k = 0$ wave functions marked in Figs. 6(a) and 6(d), respectively, one from a midgap band (shown in red) and another from the bulk CB (shown in blue). In contrast to the states from the bulk bands, whose probability density peaks near the PNR middle, the midgap state's probability density is highest by the edges (near one edge in the top sublayer and near the other end in the bottom sublayer of a given monolayer). Therefore, electronic transport in PNRs should be tunable by the manipulation of the midgap states, confined to the edges.

Based on this finding, we propose a field-effect-

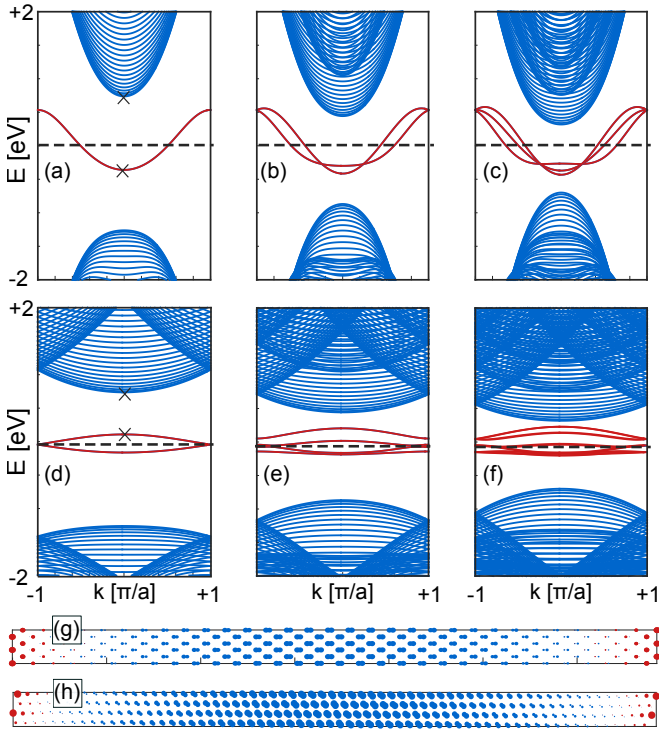


FIG. 6. Band structure of (a) monolayer, (b) bilayer, and (c) trilayer zigzag PNRs. Band structures of their skewed-armchair counterparts are shown in (d)–(f), respectively. All ribbons are 18 nm wide. (g) and (h) Probability densities of the states whose energies are marked by “x” in panels (a) and (d), respectively. The red (blue) circles denote the probability densities of the midgap (bulk) states shown by the same color in panels (a) and (d).

transistor (FET) structure shown in Fig. 7(a), where the conductance in PNRs via the midgap states (which are confined near the edges) is modulated locally by two edge gates, with voltages V_{g1} and V_{g2} . The width of the ribbons (W_R) is chosen to be 18 nm, wide enough for experimental realization yet narrow enough to be computationally feasible via atomistic TB and nonequilibrium Green’s functions (NEGF) [45]. The width of each edge gate (W_g) is 5 nm and the drain voltage (V_d) is fixed at $V_d = 0.1$ V. Figure 7(b) and (d) shows the band dispersion for zigzag and skewed armchair PNRs for $V_{g1} = -V_{g2} = +0.4$ V respectively. The applied bias strongly affects the midgap states, which have a high probability density right under the gate. The field induced by the bias shifts the bands whose wave function is localized in the upper sublayer upwards and shift the bands whose wave function is in the lower sublayer downward.

These edge gates have essentially no effect on the bulk bands. Although the midgap states have moved toward the bulk bands compared to their initial position in the gap [see Figs. 6(b) and 6(e)], the ribbon remains metallic since the Fermi level [which is fixed by the potentials on

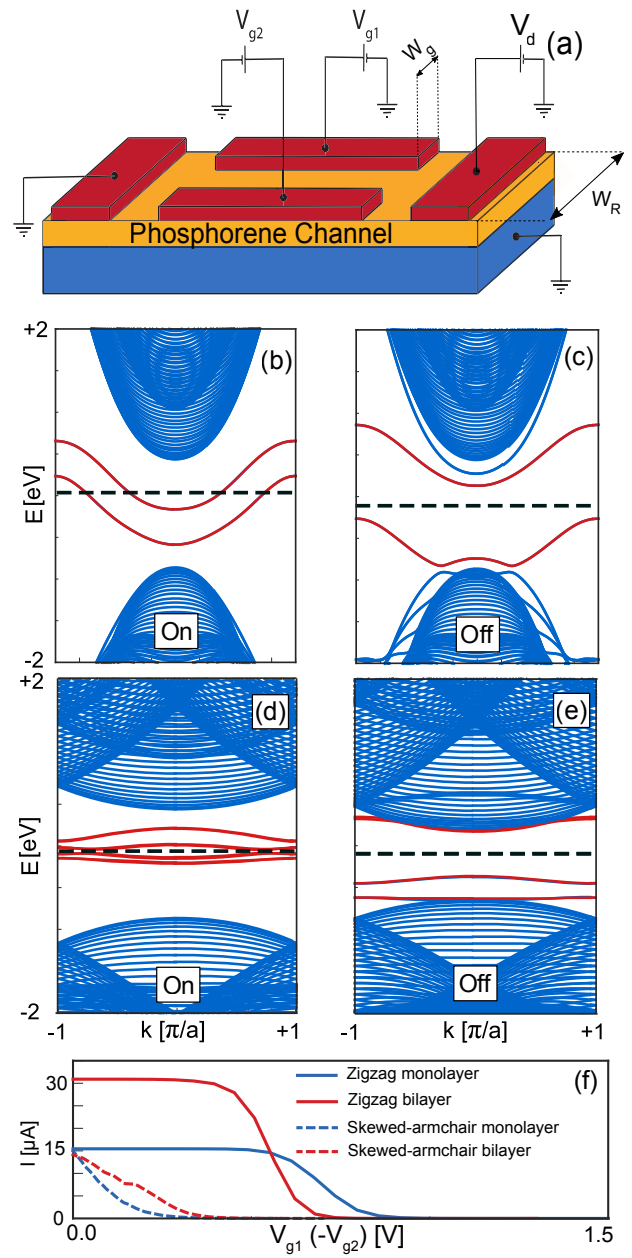


FIG. 7. (a) Schematic of the proposed dual-edge-gate field-effect structure to control the conductance in PNRs. (b) & (c) [(d) & (f)] Band structure of zigzag (skewed-armchair) bilayer PNRs under applied bias on the edge gates. Plots in (b) and (d) are for bias $V_{g1} = -V_{g2} = +0.4$ V, while in (c) and (d) $V_{g1} = -V_{g2} = +0.8$ V. Red curves represent the dispersions of the twofold degenerate midgap bands, whose wave functions are confined near the PNR edges. The dashed horizontal line represents the Fermi level. (f) Current in single and bilayer PNRs as a function of applied bias on the edge gates, indicating a transition from a conductor to an insulator. The results are limited to single and bilayer PNRs since in trilayer PNRs the van der Waals interaction between layers reduces the energy difference between the midgap states and the bulk states [see Fig. 6(c) and (f)]. As a result, bulk states are also affected by the bias of the gates and a transition to the “off” state is not accessible at room temperature in trilayer PNRs.

the source and drain on the left and right, Fig. 7(a)] still passes through the midgap bands. Increasing the bias voltages to $V_{g1} = -V_{g2} = +0.8$ V in Figs. 7(c) and 7(e) leads to a further energy separation of the midgap bands, so there are no states at the Fermi level, which denotes a transition from conducting [Fig. 6(b) and (d)] to insulating behavior [Fig. 6(c) and 6(e)].

This transition is also demonstrated by calculating the current for single and bilayer PNRs at room temperature ($T = 300^\circ\text{K}$) [Fig. 7(f)] using the ballistic NEGF formalism. [45]. At low bias on the edge gates, the current I [Fig. 7(f)] is relatively high, indicating that midgap states are crossing the Fermi level or located at the vicinity of Fermi level. As the voltage magnitude increases, the midgap states are pushed apart. Above a threshold bias on the edge gates, the current becomes vanishingly small, demonstrating a transition to an insulator [Fig. 7(f)]. This dual-edge-gate structure is compatible with current fabrication technology, as similar multigate structures were realized previously [46, 47]. Also, the topologically protected midgap states are robust against bulk vacancies [48]. A recent calculation showed that edge functionalization can lead to a dramatic flattening of the midgap-band dispersions [49], which would significantly reduce the threshold voltage required for the conductor-to-insulator transition.

V. CONCLUSION

In summary, we showed that the electron band dispersion for multilayer phosphorene transitions from

parabolic in the zigzag and massive Dirac fermion in the armchair direction at vertical electric fields below E_c to a dispersion of an anisotropic massless Dirac fermion at electric fields above E_c . We posited that this transition would be observed in quantum Hall experiments as an electric-field-dependent change in the Landau-level energy vs B : $\sim (n + 1/2)B$ below E_c , $\sim [(n + 1/2)B]^{2/3}$ at E_c , and $\sim [(n + 1/2)B]^{1/2}$ above E_c .

Moreover, we showed that PNRs feature degenerate edge states with energies belonging to midgap bands, which govern low-field conduction. We proposed a structure with dual edge gates that strongly affect the edge states but leave the bulk ones inert. The dual-edge-gate structure can induce a transition from a conducting “on” state to an insulating “off” state by moving the midgap bands away from the Fermi level, thereby realizing field-effect transistor action on PNRs.

Electric-field modulation of phosphorene and PNRs is a versatile concept that can enable access to new physics and establish a framework for further investigation of phosphorene-based devices.

VI. ACKNOWLEDGEMENT

This work was primarily supported by NSF through the University of Wisconsin Materials Research Science and Engineering Center (DMR-1121288). The work was performed using the resources of the UW-Madison Center for High Throughput Computing (CHTC).

[1] W. Lu, H. Nan, J. Hong, Y. Chen, C. Zhu, Z. Liang, X. Ma, Z. Ni, C. Jin, and Z. Zhang, *Nano Research* **7**, 853 (2014).
[2] H. Liu, A. T. Neal, Z. Zhu, Z. Luo, X. Xu, D. Tománek, and P. D. Ye, *ACS Nano* **8**, 4033 (2014).
[3] S. Zhang, J. Yang, R. Xu, F. Wang, W. Li, M. Ghufran, Y.-W. Zhang, Z. Yu, G. Zhang, Q. Qin, *et al.*, *ACS Nano* **8**, 9590 (2014).
[4] V. Tran, R. Soklaski, Y. Liang, and L. Yang, *Phys.Rev.B* **89**, 235319 (2014).
[5] Y. Jing, Q. Tang, P. He, Z. Zhou, and P. Shen, *Nanotechnology* **26**, 095201 (2015).
[6] M. Buscema, D. J. Groenendijk, S. I. Blanter, G. A. Steele, H. S. van der Zant, and A. Castellanos-Gomez, *Nano.Lett* **14**, 3347 (2014).
[7] S. P. Koenig, R. A. Doganov, H. Schmidt, A. C. Neto, and B. Oezylimaz, *App.Phys.Lett* **104**, 103106 (2014).
[8] F. Xia, H. Wang, and Y. Jia, *Nature Communications* **5** (2014).
[9] D. Çakir, C. Sevik, and F. M. Peeters, *Phys.Rev.B* **92**, 165406 (2015).
[10] D. Çakir, H. Sahin, and F. M. Peeters, *Phys.Rev.B* **90**, 205421 (2014).
[11] R. Fei and L. Yang, *Nano.Lett* **14**, 2884 (2014).
[12] R. Fei, A. Faghaninia, R. Soklaski, J.-A. Yan, C. Lo, and L. Yang, *Nano.Lett* **14**, 6393 (2014).
[13] S. Yuan, A. Rudenko, and M. Katsnelson, *Phys.Rev.B* **91**, 115436 (2015).
[14] G. Qin, Q.-B. Yan, Z. Qin, S.-Y. Yue, M. Hu, and G. Su, *Physical Chemistry Chemical Physics* **17**, 4854 (2015).
[15] Y. Cai, Q. Ke, G. Zhang, Y. P. Feng, V. B. Shenoy, and Y.-W. Zhang, *Advanced Functional Materials* **25**, 2230 (2015).
[16] T. Low, R. Roldán, H. Wang, F. Xia, P. Avouris, L. M. Moreno, and F. Guinea, *Phys.Rev.Lett* **113**, 106802 (2014).
[17] M. Elahi, K. Khaliji, S. M. Tabatabaei, M. Pourfath, and R. Asgari, *Phys.Rev.B* **91**, 115412 (2015).
[18] S. Das, W. Zhang, M. Demarteau, A. Hoffmann, M. Dubey, and A. Roelofs, *Nano.Lett* **14**, 5733 (2014).
[19] J. Kim, S. S. Baik, S. H. Ryu, Y. Sohn, S. Park, B.-G. Park, J. Denlinger, Y. Yi, H. J. Choi, and K. S. Kim, *Science* **349**, 723 (2015).
[20] C. Dutreix, E. Stepanov, and M. Katsnelson, *Phys.Rev.B* **93**, 241404 (2016).
[21] Q. Liu, X. Zhang, L. Abdalla, A. Fazzio, and A. Zunger, *Nano.Lett* **15**, 1222 (2015).

[22] T. Low, Y. Jiang, and F. Guinea, Phys.Rev.B **92**, 235447 (2015).

[23] A. Rudenko, S. Yuan, and M. Katsnelson, Phys.Rev.B **92**, 085419 (2015).

[24] A. N. Rudenko and M. I. Katsnelson, Phys.Rev.B **89**, 201408 (2014).

[25] S. Weinberg, *Gravitation and cosmology: principles and applications of the general theory of relativity*, Vol. 1 (Wiley New York, 1972).

[26] X. Zhou, R. Zhang, J. Sun, Y. Zou, D. Zhang, W. Lou, F. Cheng, G. Zhou, F. Zhai, and K. Chang, Scientific Reports **5** (2015).

[27] J. Pereira Jr and M. Katsnelson, Phys.Rev.B **92**, 075437 (2015).

[28] A. Ghazaryan and T. Chakraborty, Phys.Rev.B **92**, 165409 (2015).

[29] P. G. Harper, Proceedings of the Physical Society. Section A **68**, 874 (1955).

[30] D. Thouless, M. Kohmoto, M. Nightingale, and M. Den Nijs, Phys.Rev.Lett **49**, 405 (1982).

[31] K. Wakabayashi, M. Fujita, H. Ajiki, and M. Sigrist, Phys.Rev.B **59**, 8271 (1999).

[32] P. Wiegmann and A. Zabrodin, Phys.Rev.Lett **72**, 1890 (1994).

[33] S. Yuan, E. van Veen, M. I. Katsnelson, and R. Roldán, Phys.Rev.B **93**, 245433 (2016).

[34] Y. Hasegawa, R. Konno, H. Nakano, and M. Kohmoto, Phys.Rev.B **74**, 033413 (2006).

[35] The condition for energy levels in a magnetic field B is $S(E) = 2\pi(n + \frac{1}{2})eB$, where $S(E)$ is the area of constant-energy surface in reciprocal space [50]. Since $\rho(E) = \frac{\partial S(E)}{\partial E}$, the Landau levels are found to be $E_n \sim [(n + 1/2)B]^{2/3}$ for multilayer phosphorene at the critical electric field.

[36] P. Dietl, F. Piéchon, and G. Montambaux, Phys.Rev.Lett **100**, 236405 (2008).

[37] G. Montambaux, F. Piéchon, J.-N. Fuchs, and M. O. Goerbig, Phys.Rev.B **80**, 153412 (2009).

[38] G. Montambaux, F. Piéchon, J.-N. Fuchs, and M. Goerbig, The European Physical Journal B **72**, 509 (2009).

[39] C.-H. Park and N. Marzari, Phys.Rev.B **84**, 205440 (2011).

[40] R. Resta, Journal of Physics: Condensed Matter **12**, R107 (2000).

[41] Y. Zhang, Y.-W. Tan, H. L. Stormer, and P. Kim, Nature **438**, 201 (2005).

[42] M. M. Grujić, M. Ezawa, M. Ž. Tadić, and F. M. Peeters, Phys.Rev.B **93**, 245413 (2016).

[43] E. T. Sisakht, M. H. Zare, and F. Fazileh, Phys.Rev.B **91**, 085409 (2015).

[44] A. Carvalho, A. Rodin, and A. C. Neto, EPL (Euro-physics Letters) **108**, 47005 (2014).

[45] S. Datta, *Electronic transport in mesoscopic systems* (Cambridge university press, 1997).

[46] M. Craciun, S. Russo, M. Yamamoto, J. B. Oostinga, A. Morpurgo, and S. Tarucha, Nature Nano **4**, 383 (2009).

[47] J. Williams, T. Low, M. Lundstrom, and C. Marcus, Nature Nano **6**, 222 (2011).

[48] M. Ezawa, New Journal of Physics **16**, 115004 (2014).

[49] X. Peng, A. Copple, and Q. Wei, Journal of Applied Physics **116**, 144301 (2014).

[50] I. Lifshitz and A. Kosevich, Sov. Phys. JETP **2**, 636 (1956).